Materials and Design 64 (2014) 783–793

Contents lists available at ScienceDirect

Materials and Design

journal homepage: www.elsevier.com/locate/matdes

Technical Report

The effects of various reinforcements on dry sliding wear behaviour of AA 6061 nanocomposites

D. Jeyasimman [a], R. Narayanasamy [a,*], R. Ponalagusamy [b], V. Anandakrishnan [a], M. Kamaraj [c]

[a] Department of Production Engineering, National Institute of Technology, Tiruchirappalli, Tamil Nadu 620015, India
[b] Department of Mathematics, National Institute of Technology, Tiruchirappalli 620015, Tamil Nadu, India
[c] Department of Metallurgical and Materials Engineering, Indian Institute of Technology Madras, Chennai, Tamil Nadu 600036, India

ARTICLE INFO

Article history:
Received 16 July 2014
Accepted 15 August 2014
Available online 27 August 2014

ABSTRACT

The present work aims to investigate the dry sliding wear behaviour of AA 6061 nanocomposites reinforced with various nanolevel reinforcements, such as titanium carbide (TiC), gamma phase alumina (γ-Al_2O_3) and hybrid (TiC + Al_2O_3) nanoparticles with two weight percentages (wt.%) prepared by 30 h of mechanical alloying (MA). The tests were performed using a pin-on-disk wear tester by sliding these pin specimens at sliding speeds of 0.6, 0.9 and 1.2 m/s against an oil-hardened non-shrinking (OHNS) steel disk at room temperature. Wear tests were conducted for normal loads of 5, 7 and 10 N at different sliding speeds at room temperature. The variations of the friction coefficient and the wear rate with the sliding distances (500 m, 1000 m and 1600 m) for different normal loads and sliding velocities were plotted and investigated. To observe the wear characteristics and to investigate the wear mechanism, the morphologies of the worn surfaces were analysed using a scanning electron microscope (SEM). The formation of an oxide layer on the worn surface was examined by energy dispersive spectroscopy (EDS). The wear rate was found to increase with the load and sliding velocity for all prepared nanocomposites. Hybrid (TiC + Al_2O_3) reinforced AA 6061 nanocomposites had lower wear rates and friction coefficients compared with TiC and Al_2O_3 reinforced AA 6061 nanocomposites.

1. Introduction

Metal Matrix Composites (MMCs) have emerged as an important class of materials for structural, wear, thermal and electrical applications, primarily because of their superior strength-to-weight and strength-to-cost ratios when compared to equivalent commercial alloys. The metal matrix composite properties depend on the matrix metal, reinforcement material, reinforcement particle size and composite fabrication method [1]. The aluminium based matrix composites (AMC) have the potential to offer desirable properties, including strength, high specific stiffness and excellent wear resistance, that make them attractive for numerous applications in aerospace, automotive and military industries [2–4]. Although these composites have become one of the important lightweight materials in the last few decades, the main drawbacks of these alloys are their lower strengths at both room temperature and elevated temperatures and poor wear and corrosion resistances. Among these issues, wear is the dominant problem in industrial components, leading to a reduced lifespan. The reinforcement phase in AMCs could be as particle, continuous fibre, short fibre or whisker. Among these reinforcement phase, particle reinforced AMCs are isotropic and easier to manufacture. Lim et al. [5] found that only 1.1 vol% Al_2O_3 nanoparticles raised the wear resistance of the composites up to 1.8 times over that of magnesium matrix. Because of its low density, low melting point, high specific strength and thermal conductivity, aluminium has been reinforced with a wide variety of ceramic particulates such as Al_2O_3 [6–9], SiC [8–11], B_4C [12,13], TiB_2 [14,15] and TiC [16,17]. Among these particulates, TiC and Al_2O_3 have emerged as outstanding ceramic reinforcements because of their prominent mechanical, electrical and optical properties and wide range of applications. Jerome et al. [17] studied the effects of TiC ceramic particulate addition on the high temperature sliding wear resistance of in situ composites produced from a mixture of K_2TiF_6 and graphite powder in molten metal. They observed that the wear rate increased with an increase in applied load and decreased with an increase of the weight percentage of TiC. Both monolithic and composites showed a resistance to thermal softening through the formation of an oxidation transfer layer. In their study on the dry sliding wear behaviour of Al_2O_3 particle reinforced 6061 alloy, Zhang and Alpas [6], showed that there were three wear regimes:

* Corresponding author. Tel.: +91 431 2503504; fax: +91 431 2500133.
E-mail addresses: jeyasimman76@gmail.com (D. Jeyasimman), narayan@nitt.edu (R. Narayanasamy), rpalagu@nitt.edu (R. Ponalagusamy), krishna@nitt.edu (V. Anandakrishnan), kamaraj@iitm.ac.in (M. Kamaraj).

http://dx.doi.org/10.1016/j.matdes.2014.08.039
0261-3069/

Table 1
The amount of the pure elemental powders required to prepare the AA 6061 alloy.

Element	Si	Fe	Cu	Mn	Mg	Cr	Zn	Ti	Al
wt.%	0.600	0.700	0.275	0.150	1.000	0.195	0.250	0.150	Balance

at low loads (<10 N), the wear rate of the composite was two orders lower than the matrix alloy; at intermediate loads up to 230 N, the wear rates were similar; and at higher loads (>230 N), a transition to severe wear occurred in both the alloy and the composite, although the composite showed an impedance in the transition until higher loads. The objective of two reinforcements is to take advantage of the superior properties of both materials without compromising on the weakness of either [18]. The wear properties of hybrid particulate reinforced composites (Al/(Al_2O_{3p} + SiC_p)) are more excellent than those of the single reinforcement reinforced composites (Al/Al_2O_{3p} and Al/SiC_p) [19]. Gurcan and Baker [20] investigated the dry sliding wear behaviour of AA 6061/(Al_2O_{3f} + SiC_p) hybrid composites and reported that hybrid composites had better wear resistance than that of single Al_2O_{3f} and /SiC_p reinforced AA 6061 composites. Park [21] also investigated and reported that hybrid composites (Al/Al_2O_{3f} + SiC_w) had higher wear resistance than those of Al/SiC_w and Al/Al_2O_{3f} composites. Similar result were obtained by Sharifi and Karimzadeh [22] through dry sliding wear behaviour of Al/Al_2O_3/AlB_{12} hybrid composites and Suresha and Sridhara [23] through dry sliding wear behaviour of Al/SiC_p/Gr_p hybrid composites. Ravindran et al. [24,25] investigated the wear rate and friction response of a hybrid aluminium metal matrix composite reinforced with 5 wt.% SiC and graphite. They observed that the addition of the hybrid reinforcement improves the wear resistance of aluminium composites significantly. Umanath et al. [26] found that a high volume fraction of reinforcement, low applied load, low rotational speed and high counter face material hardness reduced the wear rate of Al 6061/SiC/Al_2O_3 hybrid composites.

The synthesis, consolidation behaviour, sinterability, green compression strength and Vickers hardness of AA 6061 nanocomposites reinforced with TiC, gamma phase alumina and hybrid (TiC + Al_2O_3) nanoparticles with various weight percentages (0, 0.5, 1.0, 1.5 and 2.0) were studied and investigated in our earlier studies [27–29]. However, detailed investigations have not yet been conducted for a comparative study on the effect of TiC, alumina and hybrid (TiC + Al_2O_3) nanolevel ceramic reinforcements on the dry sliding wear behaviour of the AA 6061 nanocomposites.

The present research primarily aimed to study and investigate the dry sliding wear behaviour of AA 6061 nanocomposites with various nanolevel ceramic reinforcements such as TiC, Al_2O_3 and hybrid (TiC + Al_2O_3) via mechanical alloying (MA) followed by a conventional consolidation technique. The study of wear rate and friction depends on applied load, environmental temperature, sliding speed, type of materials, relative humidity and system rigidity. Among these parameters, sliding speed and applied normal load are found to have more influenced on wear rate [30]. The effects of normal loads, sliding velocity and sliding distance on the obtained nanocomposites were investigated in this research.

2. Experimental details

2.1. Nanocomposites fabrication

AA 6061 alloy was produced by blending the highly pure (greater than 99%) elemental powders of aluminium, silicon, magnesium, iron, copper, zinc, chromium, titanium and manganese. The amount of the pure elemental powders required to prepare the AA 6061 alloy are shown in Table 1. As-received pure aluminium powder with an average particle size of 7–15 μm was used as the major matrix material, and the remaining alloying elements had an average particle size of less than 45 μm. Alfa Aesar, USA, supplied all powders. AA 6061-2 wt.% TiC, AA 6061-2 wt.% Al_2O_3 and AA 6061-2 wt.% hybrid (TiC + Al_2O_3) nanocomposite powders were prepared from the pure elemental powders. The titanium carbide (TiC) with an average particle size of less than 200 nm with more than 95% purity, which was supplied by Sigma Aldrich, China, and the gamma phase alumina nanoparticles (γ-Al_2O_3) of 99.5% purity with an average particle size (APS) of 40–50 nm, which were supplied by Alfa Aesar, USA, were used as reinforcements. Thirty grams of AA 6061-2 wt.% TiC, AA 6061-2 wt.% Al_2O_3 and AA 6061-2 wt.% hybrid (1 wt.% TiC + 1 wt.% Al_2O_3) powder mixture and 300 grams of steel balls (nine balls each 20 mm diameter with a mass of 33.5 g) were chosen, maintaining a ball to powder ratio of 10:1 for the processing of the nanocomposites. Toluene was used as a process control agent (PCA) to avoid excessive cold welding of powder particles. The plate speed of the mill was set to 100 rpm and the corresponding bowl/vial speed was 280 rpm. Milling was performed for 30 h to reach the steady state condition. To avoid overheating, the high-energy ball milling stopped periodically every 20 min and then resumed. The milled composites are designated as AA 6061-2 wt.% TiC, AA 6061-2 wt.% Al_2O_3 and AA 6061-2 wt.% hybrid (TiC + Al_2O_3) nanocomposites. The milled powders were consolidated using a double action compaction die in a hydraulic press (Insmart Systems, Hyderabad, India) with a capacity of 40 tons at room temperature. Cylindrical compacts of 10 mm diameter and 15 mm height were mechanically pressed with a compaction pressure of 500 MPa. Zinc-Strearate was used as a lubricant between the inner surfaces of the cylindrical die to reduce the friction. The green cylindrical compacts were degassed at 350 °C for 1 h and then sintered for 2 h at a temperature of

Table 2
Mechanical properties of AA 6061 nanocomposites reinforced with various nanolevel ceramic reinforcements Refs. [27–29].

Sl. no	Composition	Green density (ρ_g) (g/cm^3)	Sintered density at 798 K (ρ_s) (g/cm^3)	Green compressive strength (MPa)	Ultimate incremental compressive strength (MPa)	Vickers hardness ($HV_{0.5}$) for various sintering temperatures (MPa)	
						303 K	798 K
1	AA 6061-2 wt.% TiC [27]	2.53	2.57	233	539	786 ± 22	1024 ± 18
2	AA 6061-2 wt.% Al_2O_3 [28]	2.50	2.54	176	580	604 ± 13	695 ± 10
3	AA 6061-2 wt.% hybrid (TiC + Al_2O_3) [29]	2.46	2.50	211	564	843 ± 21	912 ± 27

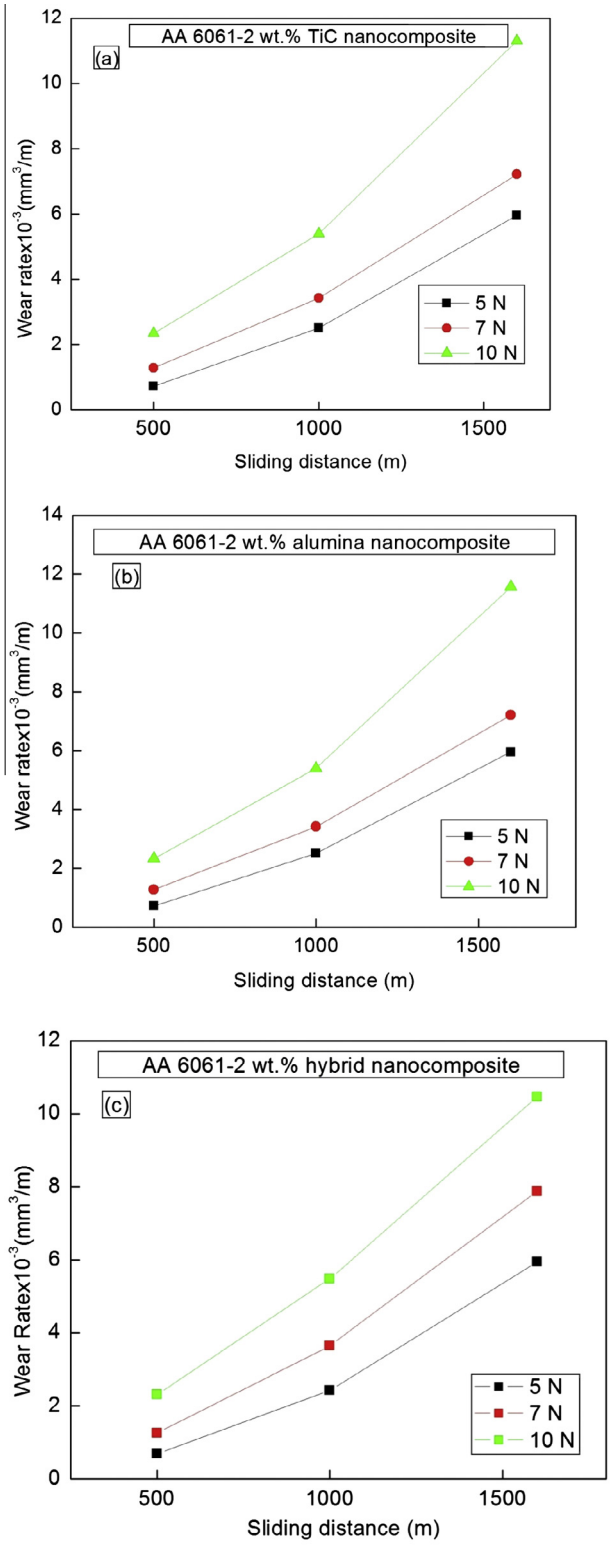

Fig. 1. Variation in wear rate as a function of sliding distance for all applied loads at a sliding velocity of 0.6 m/s (a) AA 6061-2 wt.% TiC; (b) AA 6061-2 wt.% Al_2O_3; (c) AA 6061-2 wt.% hybrid (TiC + Al_2O_3).

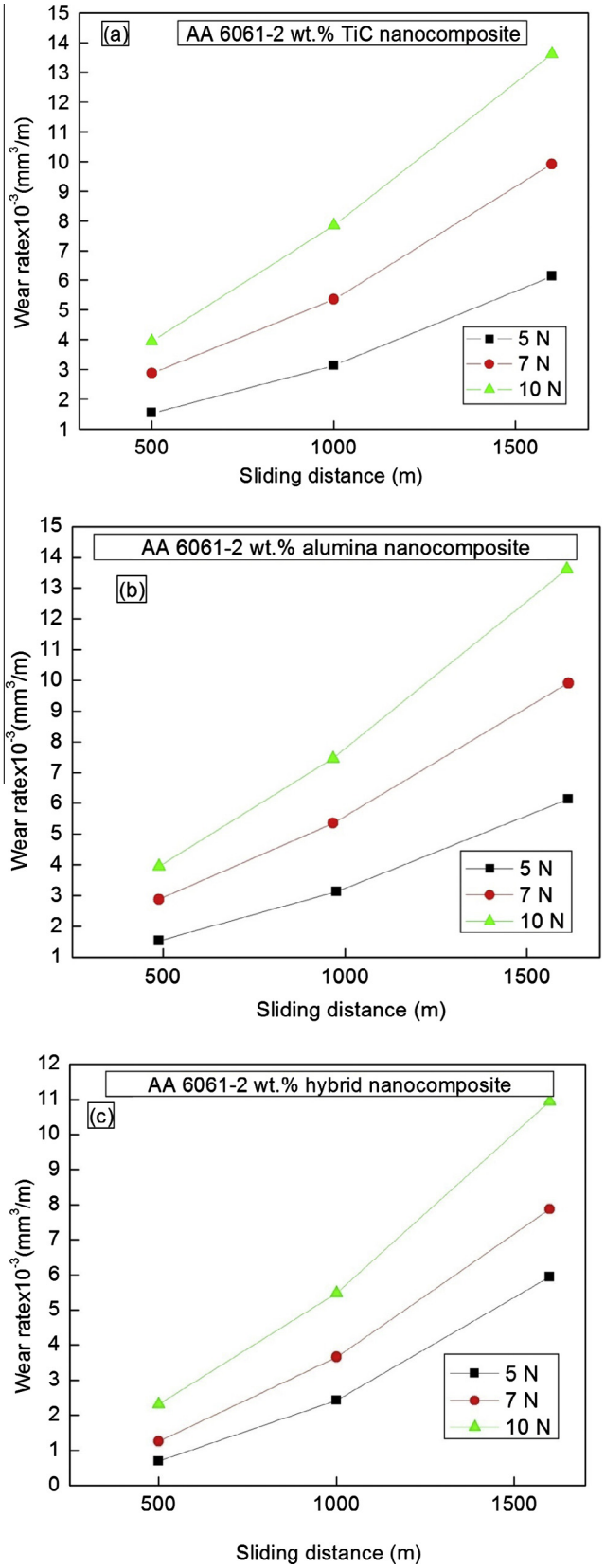

Fig. 2. Variation in wear rate as a function of sliding distance for all applied loads at a sliding velocity of 0.9 m/s (a) AA 6061-2 wt.% TiC; (b) AA 6061-2 wt.% Al_2O_3; (c) AA 6061-2 wt.% hybrid (TiC + Al_2O_3).

525 °C under reducing nitrogen atmosphere. The densities of the green and sintered cylindrical specimens were estimated using the Archimedes principle. The results were averaged over three independent measurements. The estimated error in the density measurements was less than ±1%. The mechanical properties of the AA 6061 alloy reinforced with 2 wt.% TiC, Al_2O_3 and hybrid (TiC + Al_2O_3) nanocomposites are shown in Table 2.

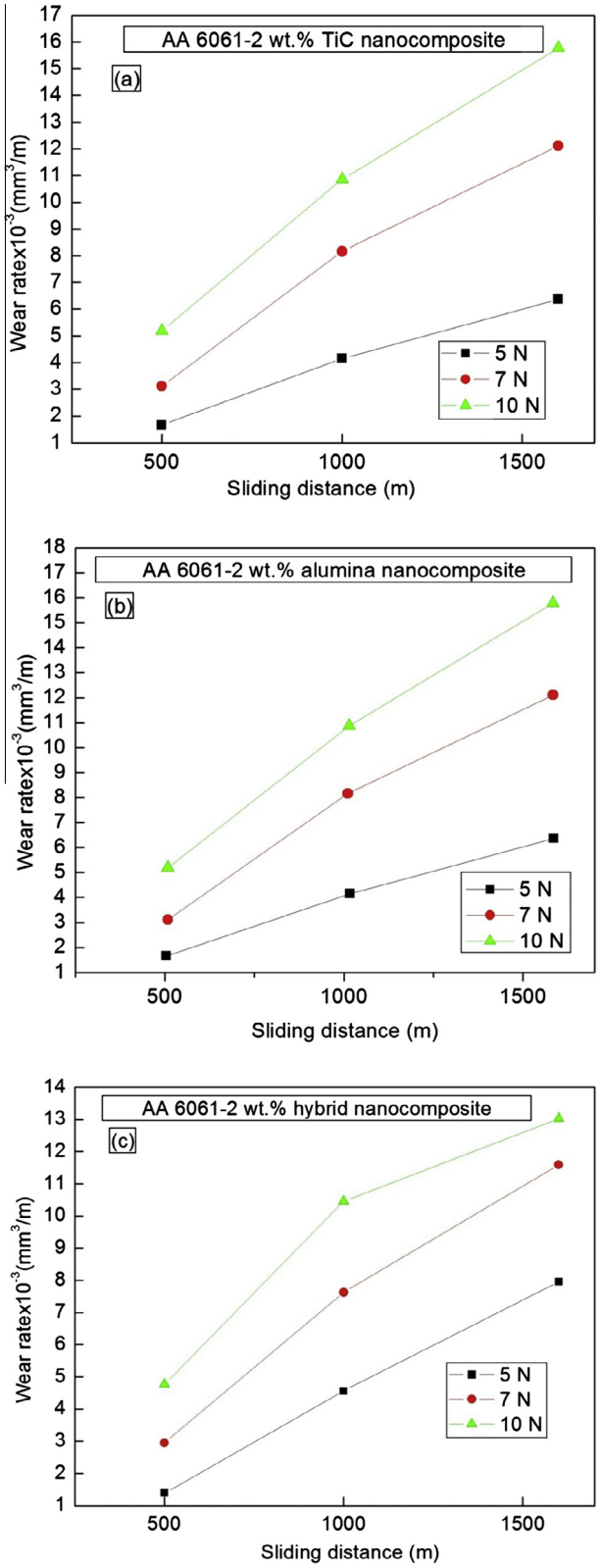

Fig. 3. Variation in wear rate as a function of sliding distance for all applied loads at a sliding velocity of 1.2 m/s (a) AA 6061-2 wt.% TiC; (b) AA 6061-2 wt.% Al_2O_3 and (c) AA 6061-2 wt.% hybrid (TiC + Al_2O_3).

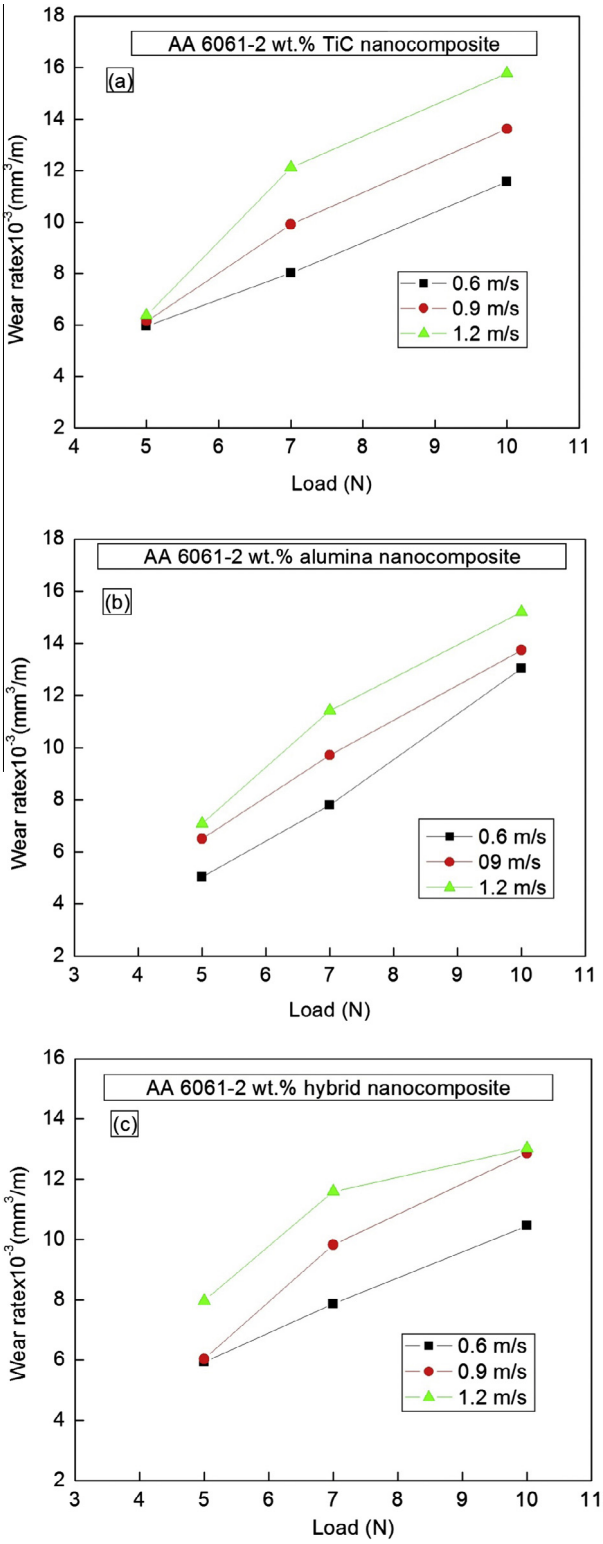

Fig. 4. Variation in wear rate as a function of load for all sliding velocities (a) AA 6061-2 wt.% TiC; (b) AA 6061-2 wt.% Al_2O_3 and (c) AA 6061-2 wt.% hybrid (TiC + Al_2O_3).

2.2. Preparation of pins and disc for wear testing

The pins with 10 mm diameter and 15 mm height were used for wear testing. The end of each pin's surface was not allowed to have any burrs and sharp corners because of possible damaged while sliding on the disc surface. The contact surfaces of the pins were smoothed using 600-grit SiC paper and subsequently cleaned with acetone. The surfaces of the pins were checked for perpendicularity and flatness to seat with the disc surface to maintain 100% contact

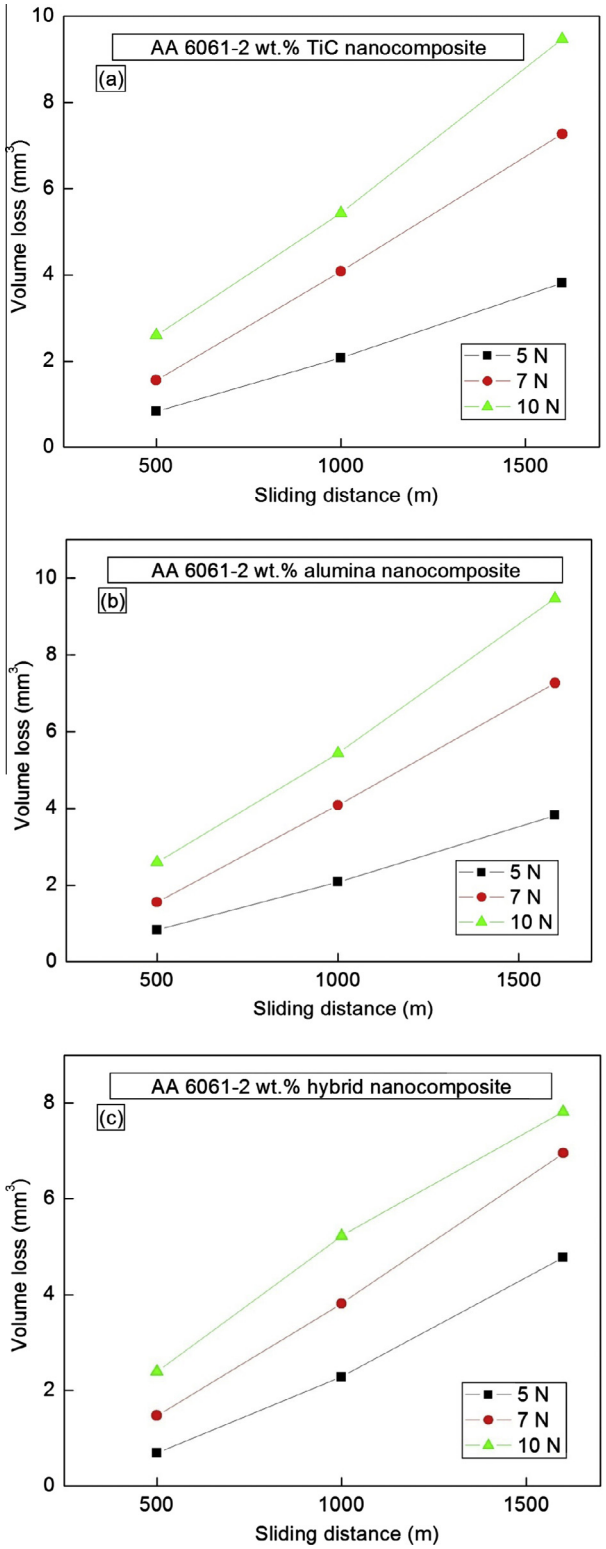

Fig. 5. Variation in volume loss as a function of sliding distance for all normal applied loads at a sliding velocity of 1.2 m/s (a) AA 6061-2 wt.% TiC; (b) AA 6061-2 wt.% Al_2O_3 and (c) AA 6061-2 wt.% hybrid (TiC + Al_2O_3).

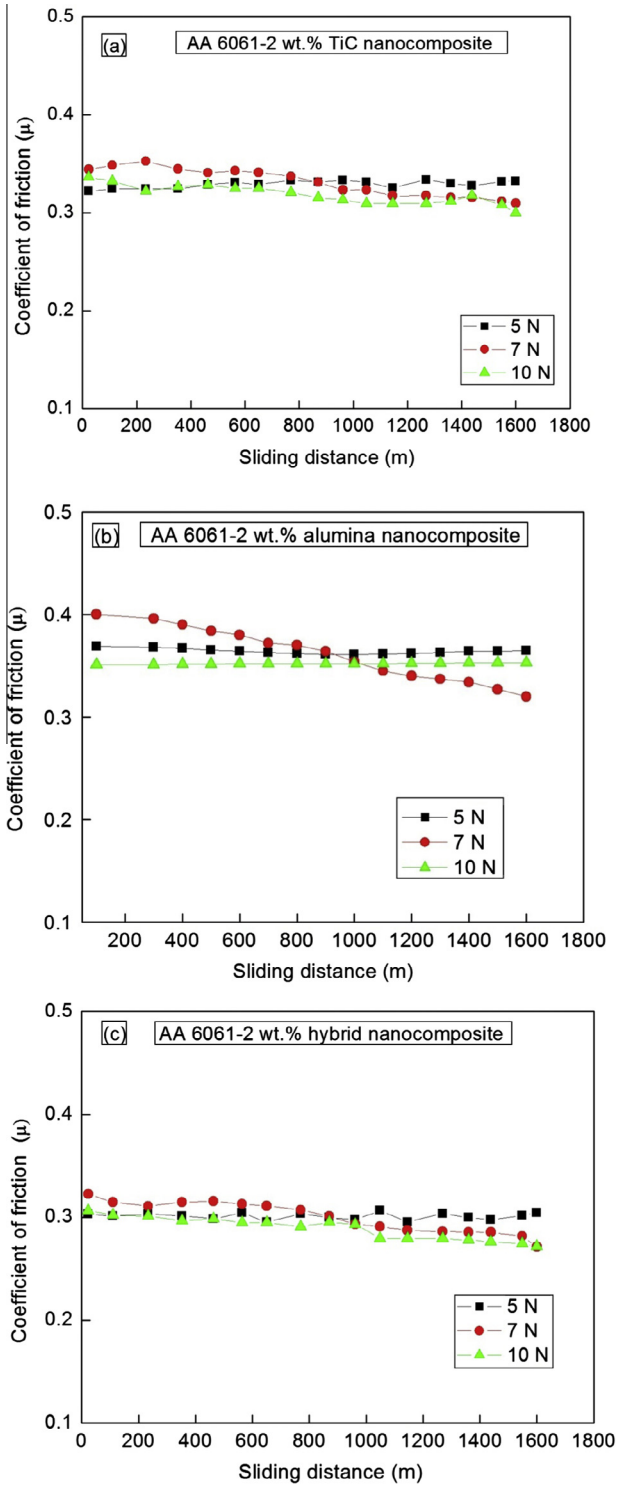

Fig. 6. Variation in the coefficient of friction as a function of sliding distance for all normal applied loads at a sliding velocity of 0.6 m/s (a) AA 6061-2 wt.% TiC; (b) AA 6061-2 wt.% Al_2O_3 and (c) AA 6061-2 wt.% hybrid (TiC + Al_2O_3).

between the samples and the disc surface. The surface roughness value of the pins was measured and maintained at 0.8 μm (Ra) to obtain uniform wear results. The disc is made of oil hardened non-shrinking steel that had been oil hardened to 62 HRC. The disc surface was ground with 600-grit SiC paper for a few minutes to remove accumulated particles on the wear track and finally cleaned with acetone. The disc surface roughness was also measured and recorded as 0.45 μm. After the grinding, fine polishing was performed with a mechanical polishing machine as per ASTM: E3 using a diamond paste having particle sizes of 1 μm.

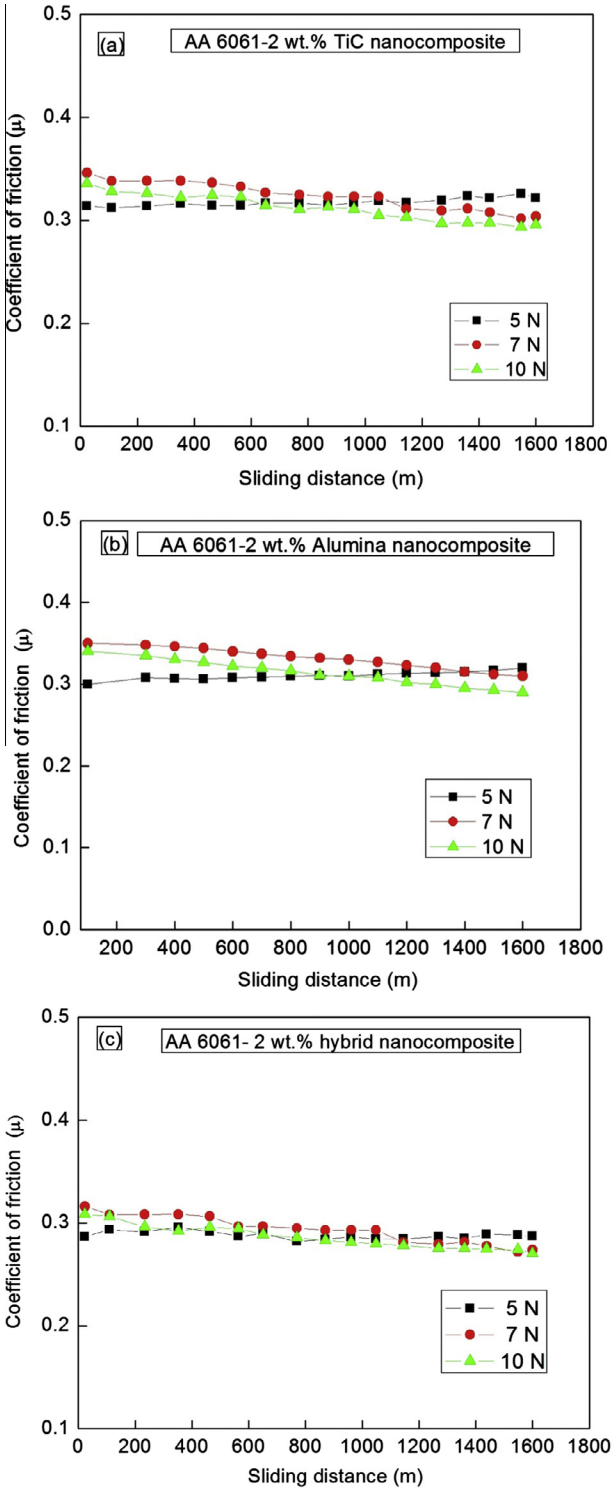

Fig. 7. Variation in the coefficient of friction as a function of sliding distance for all normal applied loads at a sliding velocity of 0.9 m/s (a) AA 6061-2 wt.% TiC; (b) AA 6061-2 wt.% Al_2O_3 and (c) AA 6061-2 wt.% hybrid (TiC + Al_2O_3).

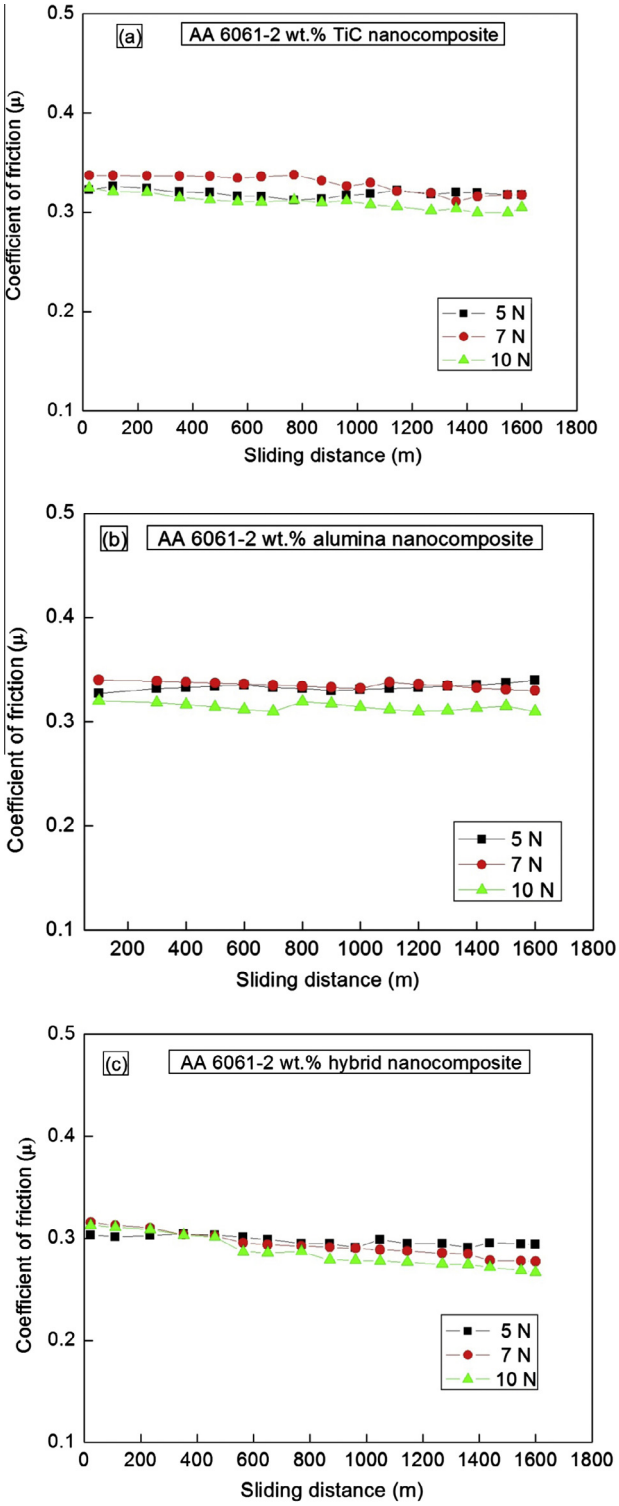

Fig. 8. Variation in the coefficient of friction as a function of sliding distance for all normal applied loads at a sliding velocity of 1.2 m/s (a) AA 6061-2 wt.% TiC; (b) AA 6061-2 wt.% Al_2O_3 and (c) AA 6061-2 wt.% hybrid (TiC + Al_2O_3).

2.3. Wear test

Wear behaviour tests were conducted in air at a 30 °C room temperature according to ASTM: G99 in a DUCOM pin-on-disc wear-testing apparatus. The prepared nanocomposite samples were used as pins and were tested by sliding them on a counter face OHNS steel disc. The samples were checked and maintained at 100% of surface contact with the disc surface. The mass of the pins was measured using a sensitive electronic balance having an accuracy of ±0.1 mg. The experiments were conducted under the normal loads of 5 N, 7 N and 10 N at three different sliding velocities of 0.6 m/s, 0.9 m/s and 1.2 m/s for a sliding distance up to 1600 m [31,32].

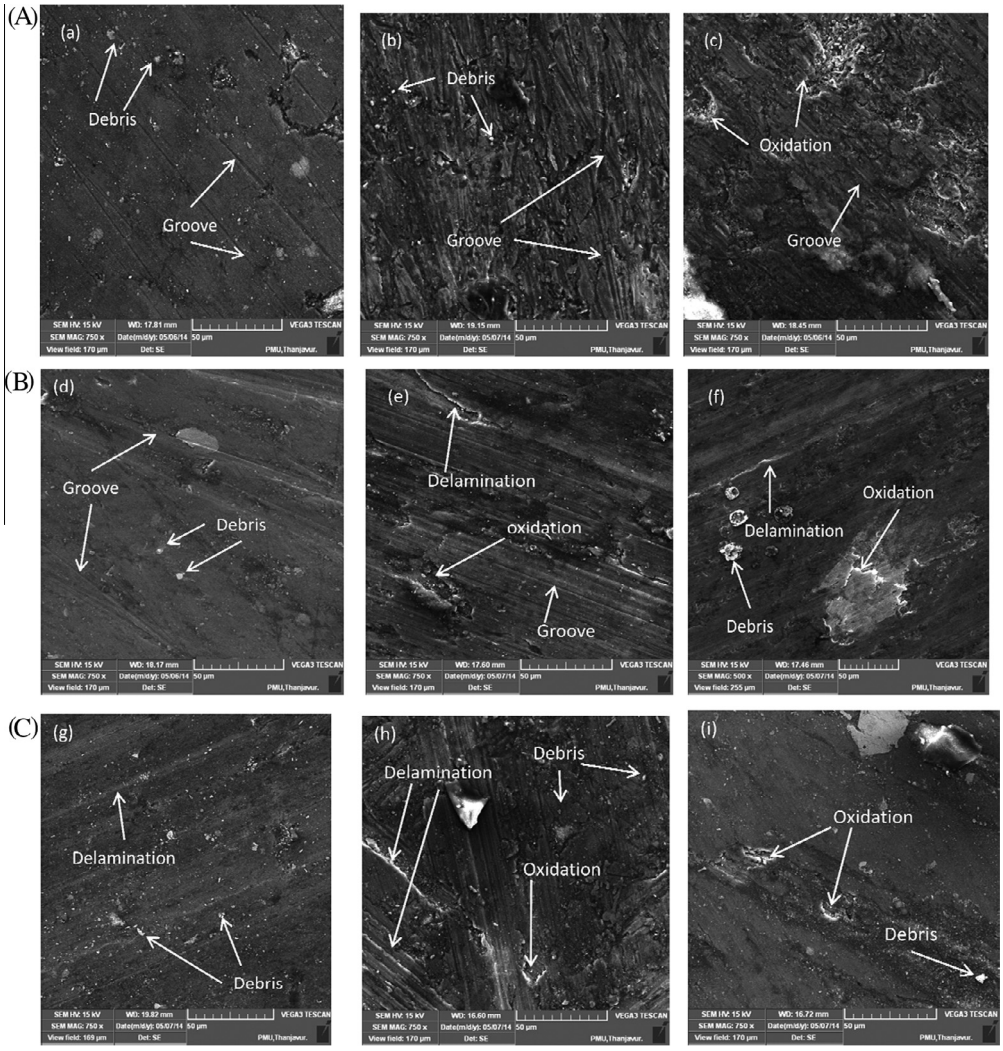

Fig. 9. Worn surface morphologies of AA 6061-2 wt.% TiC nanocomposites (A) at a velocity of 0.6 m/s; (B) at a velocity of 0.9 m/s; (C) at a velocity of 1.2 m/s; (a) 5 N; (b) 7 N; (c) 10 N; (d) 5 N; (e) 7 N; (f) 10 N; (g) 5 N; (h) 7 N and (i) 10 N.

The mass losses were calculated at every interval of sliding distance for different normal loads with respect to various sliding velocities. An *X*–*Y* plotter attached to the tester continuously recorded the coefficient of friction.

$$\text{The coefficient of friction is } \mu = \left(\frac{F}{P}\right) \tag{1}$$

where *F* is the frictional force measured by the tester and *P* is the normal load on the specimen. The volume loss due to the wear test was calculated from the weight loss according to the following equation [33]:

$$\text{Volume loss } (\text{mm}^3) = \left(\frac{\text{Weight loss (g)}}{\text{Density (g/mm}^3)}\right) \times 1000 \tag{2}$$

The wear tests were conducted five times for every pin and the obtained data were represented by the average value together with error bars. The wear rate was calculated from the following expression:

$$\text{Wear rate } (\text{mm}^3/\text{m}) = \left(\frac{\text{Volume loss } (\text{mm}^3)}{\text{Sliding distance (m)}}\right) \times 1000 \tag{3}$$

The morphologies of all the pins' worn out surfaces after the wear tests were analysed using a scanning electron microscope ((TESCAN model VEGA 3 LMU). Energy dispersive spectroscopy (EDS) analysis of the worn surfaces was also performed using a JEOL JEM 2100F field emission scanning electron microscope (FESEM) with an EDAX facility.

3. Results and discussion

3.1. Effect of sliding distance and normal applied load on the wear rate

The changes in wear rates for the AA 6061 reinforced with TiC, Al_2O_3 and hybrid (TiC + Al_2O_3) nanocomposites are plotted against sliding distance in Figs. 1–3, which show a greater slope of wear rate for the 10 N normal loads compared to the 5 N and 7 N normal loads for sliding velocities of 0.6, 0.9 and 1.2 m/s. As shown in Fig. 1, the wear rate increases linearly with sliding distances; oxidation did not happen during the sliding action of the pin against the disc surface for the 0.6 m/s sliding velocity. As shown in Fig. 2, the wear rate is not linear; the changes in wear rate decrease from sliding distances of 500 m to 1000 m and slightly increase after 1000 m. Oxidation happened at a 0.9 m/s sliding velocity from 500 m to 1000 m. After 1000 m, the oxidation layer occurred because of the sliding action of the pin against the disc surface. Fig. 3 shows that the changes in wear rate increased from 500 m to 1000 m for the normal loads of 5 N and 7 N at a 1.2 m/s sliding

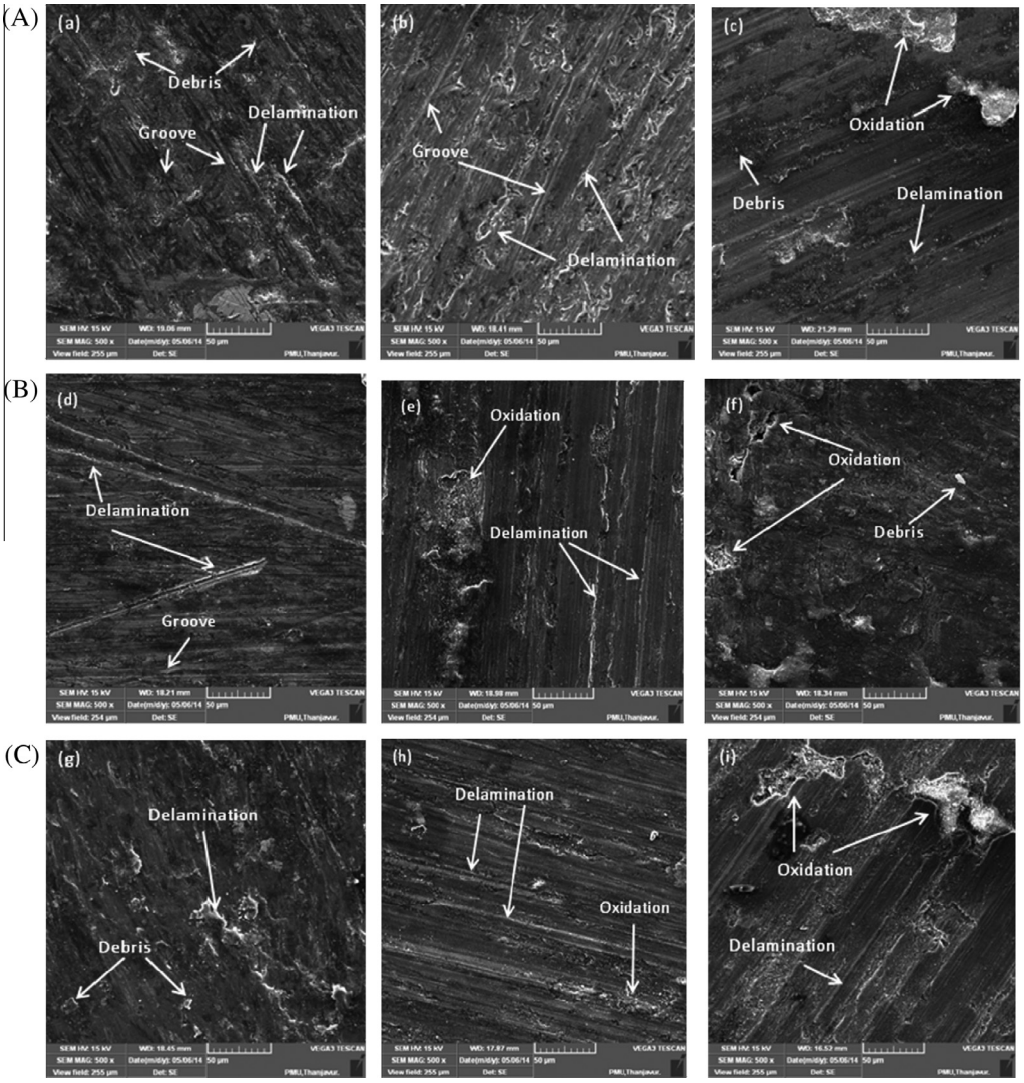

Fig. 10. Worn surface morphologies of AA 6061-2 wt.% Al_2O_3 nanocomposites (A) at a velocity of 0.6 m/s; (B) at a velocity of 0.9 m/s; (C) at a velocity of 1.2 m/s; (a) 5 N; (b) 7 N; (c) 10 N; (d) 5 N; (e) 7 N; (f) 10 N; (g) 5 N; (h) 7 N and (i) 10 N.

velocity, but changes in wear rate decreased for the normal load of 10 N at a 1.2 m/s sliding velocity. After the 1000 m sliding distance, changes in wear rate decreased irrespective of normal load. Severe oxidation occurred when the pin was operated with a normal load of 10 N at a 1.2 m/s sliding velocity. As shown in Figs. 1–3, the higher wear rate was observed at the higher normal load (10 N) at the high sliding velocity (1.2 m/s) for the AA 6061–2 wt.% TiC, Al_2O_3 nanocomposites, and the wear rate was comparatively less for the AA 6061-2 wt.% hybrid (TiC + Al_2O_3) nanocomposite.

3.2. Effect of normal applied load and sliding velocities on wear rate

Fig. 4 shows that the wear rate increases with respect to the applied load as a function of sliding velocities. For the AA 6061-2 wt.% TiC nanocomposite, the low load (5 N) shows almost same wear rate for all sliding velocities. However, a higher wear rate was obtained for the higher loads (7 N and 10 N). For the AA 6061-2 wt.% TiC and AA 6061-2 wt.% Al_2O_3 nanocomposites, the changes in wear rate increased with increasing sliding velocity and load. For the AA 6061-2 wt.% hybrid nanocomposites, the changes in wear rate were less with increasing sliding velocity and load compared with TiC and Al_2O_3 reinforced AA 6061 nanocomposites.

3.3. Effect of sliding distances and normal applied load on volume loss

Fig. 5 shows the variation in volume loss with all loads and all sliding distances at a sliding velocity of 1.2 m/s. Volume loss linearly increased with increasing loads and sliding distances for all prepared nanocomposites. Volume loss was low for the AA 6061-2 wt.% hybrid nanocomposites compared with the AA 6061–2 wt.% TiC and the AA 6061-2 wt.% Al_2O_3 nanocomposites.

3.4. Effect of sliding velocities and normal load on the coefficient of friction

Figs. 6–8 show the variations in the coefficient of friction with varying sliding distances and varying loads for AA 6061-TiC, Al_2O_3 and hybrid (TiC + Al_2O_3) nanocomposites. The average friction coefficient values for TiC, Al_2O_3 and hybrid (TiC + Al_2O_3) reinforced AA 6061 nanocomposites at a sliding velocity of 0.6 m/s were 0.34, 0.37 and 0.31, respectively (Fig. 6). Fig. 7 shows that the average friction coefficient values for TiC, Al_2O_3 and hybrid (TiC + Al_2O_3) reinforced AA 6061 nanocomposites at a velocity of 0.9 m/s were 0.33, 0.34 and 0.30, respectively. At a higher velocity of 1.2 m/s, the average friction coefficient values decreased to 0.32, 0.33 and 0.29 for TiC, Al_2O_3 and hybrid reinforced AA 6061 nano-

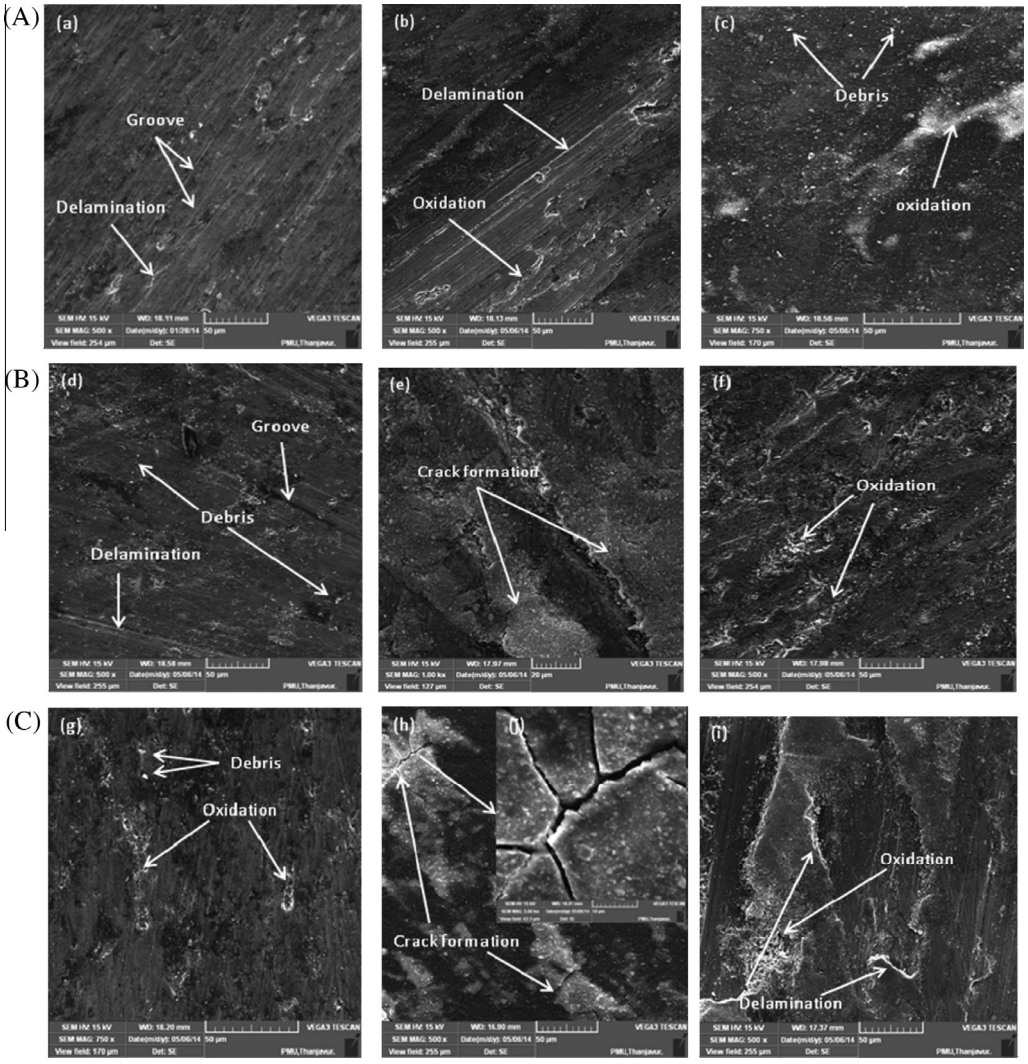

Fig. 11. Worn surface morphologies of AA 6061-2 wt.% hybrid (TiC + Al_2O_3) nanocomposites (A) at a velocity of 0.6 m/s; (B) at a velocity of 0.9 m/s; (C) at a velocity of 1.2 m/s; (a) 5 N; (b) 7 N; (c) 10 N; (d) 5 N; (e) 7 N; (f) 10 N; (g) 5 N; (h) 7 N; (i) 10 N and (j) magnified view of crack formation.

composites, respectively (Fig. 8). Hence, the average coefficient friction value decreased with increasing sliding velocity for all prepared nanocomposites. Hybrid (TiC + Al_2O_3) reinforced AA 6061 nanocomposites had a lower friction coefficient compared with TiC and Al_2O_3 reinforced AA 6061 nanocomposites. The friction coefficient fluctuates around the mean level and decreases as the sliding progresses. The variation of the coefficient of friction may be because of improper contact between the pin and the disc. Comparing the three different sliding velocities of 0.6 m/s, 0.9 m/s and 1.2 m/s, a lower coefficient of friction was recorded at the higher sliding velocity for all loads. The coefficient of friction decreased with sliding velocity with respect to the sliding distance. The decreasing trend is observed until the 1600 m sliding distance for all loads at the different sliding velocities. The normal load of 7 N produced a higher coefficient of friction compared with the 5 N and 10 N normal loads. The friction coefficient curves are consistent with previous research [32,34].

For different load conditions at a low sliding velocity (0.6 m/s), the variation in the coefficient of friction is high during the initial stages of sliding and reduces with sliding distance, as observed in Fig. 6. This variation in the coefficient of friction is associated with the wear mechanism. The interactions of asperities in the surfaces influence the coefficient of friction, which is varying in the specific range during the sliding period [34,35]. However, for the sliding velocities of 0.9 and 1.2 m/s, the variations in the coefficient of friction among the different load conditions are very low, as shown in Figs. 7 and 8. This phenomenon of low variation in the coefficient of friction for a higher velocity is because of the formation of an oxide layer, which exhibits in higher load and higher sliding velocity conditions.

3.5. Wear mechanism of worn surfaces

Three various wear mechanisms, namely, abrasion, delamination and oxidation, were observed during wear testing. Figs. 9–11 show the scanning electron microscope (SEM) images of the worn surfaces of AA 6061-TiC, Al_2O_3 and hybrid (TiC + Al_2O_3) nanocomposites under different applied loads at various sliding velocities. The worn surfaces of the AA 6061-TiC, AA 6061-Al_2O_3 and AA 6061-hybrid (TiC + Al_2O_3) nanocomposites were examined through SEM images to determine the effect of various parameters of wear, namely, sliding velocity, sliding distance, abrasive particle size and normal load, on the worn surface morphology of the composite specimen under the room temperature condition.

3.5.1. Abrasion

At a low load of 5 N, abrasion is the dominant wear mechanism as numerous grooves and scratches are evident parallel to the slid-

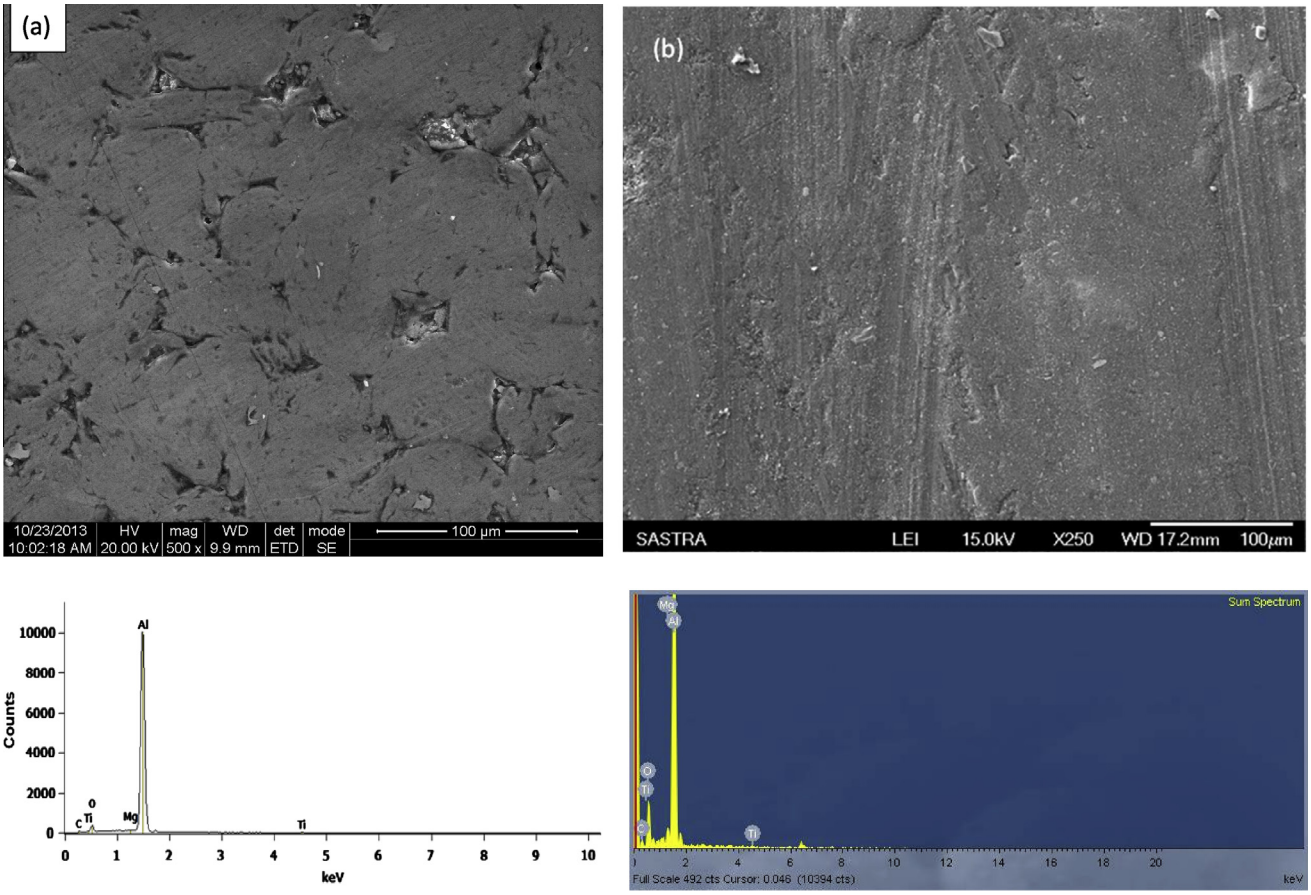

Fig. 12. (a) Energy dispersive spectroscopy (EDS) of the surface of the AA 6061-2 wt.% hybrid (TiC + Al_2O_3) nanocomposite sintered sample (before wear test) and (b) energy dispersive spectroscopy (EDS) of the worn surface of the AA 6061-2 wt.% hybrid (TiC + Al_2O_3) nanocomposites at a 1.2 m/s sliding velocity for a sliding distance of 1600 m under a 5 N load.

ing direction. For all prepared nanocomposites at all sliding velocities, debris and grooves were identified at a normal load of 5 N (Figs. 9–11(a), (d) and (g)). The worn out surfaces of the specimens were covered with grooves parallel to the sliding direction. Hard asperities on the steel counter face or hard particles in between the pin and the disc plough or cut into the pin causing wear by the removal of small fragments or ribbon-like strips of material, typical features associated with abrasive wear [36]. The deeper grooves indicate a higher degree of penetration by hard counter face asperities. The well-defined deep grooves were identified for the TiC and alumina reinforced nanocomposites. These well-defined grooves at a lower speed change to shallower scratches at higher speeds because of plastic deformation. Shallower scratches were identified in the hybrid reinforced nanocomposites (Fig. 11(a)).

3.5.2. Delamination

At a low load of 5 N, slight delamination is noticeable for all prepared nanocomposites. As the load increases, the signs of plastic deformation begin to appear, leading to severe delamination, as shown in Figs. 9–11. Simultaneously, the wear track on the steel disc became covered with a visible layer of transferred material, the thickness of which grew with increasing sliding speed. The asperities of the softer surface are deformed by the asperities of the OHNS steel counter face. This deformation induces shear deformation near the subsurface region of a softer material, thereby creating microcracks in this region. Fragments then detach from the pin surface in the form of wear debris. This behaviour is commonly known as delamination wear [37]. The wear debris formation was observed at low sliding speeds based on a delamination theory. The adhesive wear, fatigue wear and fretting wear formation processes happened because of this mechanism. If the microstructure of a material contains a hard particle, crack nucleation started around the hard particle while it was sliding against another surface. Figs. 9–11(b), (e) and (h) show that appreciable delamination occurred when the pins were sliding with high loads at higher sliding velocities. Fig. 11(e) and (h) show that the formation of cracks perpendicular to the sliding direction was much more evident for severe delamination.

3.5.3. Oxidation

The dominant wear mechanism under the load of 10 N is oxidation. The composites generally exhibit better wear resistance because of their superior load bearing capacity and ability to maintain a stable oxide film, which protects against metal-to-metal contact with the OHNS steel counter face during sliding [38]. Figs. 9–11(c), (f) and (i) show clearly the presence of an oxide film, and the relative motion between the pins and the OHNS steel disc surface generates frictional heat, which significantly affects the wear rate of pins. This oxide layer prevented metal (pins) to metal (OHNS steel disc) contact, leading to a lower wear rate [7,38]. The formation of an oxide layer on the worn surface was examined by energy dispersive spectroscopy (EDS) and the EDS was compared with the nanocomposite before the wear test in Fig. 12. From the EDS of the AA 6061-2 wt.% hybrid nanocomposite at 1.2 m/s sliding velocity for a sliding distance of 1600 m under a 5 N load

(Fig. 12(b)), the appearance of a high oxygen peak confirmed the oxidation. The absence of iron indicates that the material's transition by adhesion did not occur. This effect occurs when the applied load is low (5 N); hence, no plastic deformations occur in the worn surface [39,40].

4. Conclusions

In the present research, the effect of various nanolevel reinforcements, such as TiC, Al_2O_3 and hybrid (TiC + Al_2O_3) reinforced AA 6061 nanocomposites, on dry sliding wear behaviour was investigated. Based on results of the present work, the following conclusions can be made:

For a given load, the volume loss and wear rate increased with increasing sliding velocity and sliding distance for all nanocomposites. The increase of wear rate and volume loss was low in the case of the hybrid reinforced AA 6061 nanocomposite compared with the TiC and Al_2O_3 reinforced AA 6061 nanocomposites. The coefficient of friction decreased with sliding velocity and sliding distance. The normal applied load of 7 N produced a higher coefficient of friction compared to loads of 5 N and 10 N. The various wear mechanisms, namely, abrasion, delamination and oxidation, were established for all prepared nanocomposites from worn surface morphologies. Oxidation was confirmed from the EDS of the worn surface of the AA 6061-2 wt.% hybrid nanocomposite. The addition of the hybrid ceramic nanolevel reinforcement (TiC + Al_2O_3) in the AA 6061 matrix enhanced the wear resistance compared with the individual nanolevel reinforcements.

Acknowledgements

The authors wish to express their gratitude to the General Manager and the Joint General Managers, Heavy Alloy Penetrator Project (HAPP), Tiruchirappalli, Tamilnadu, India, for permitting them to utilise the powder metallurgy shop facilities for the present work.

References

[1] Manoj Kumar BV, Basu Bikramjit, Murthy VSR, Gupta Manoj. The role of Tribo chemistry on fretting wear of Mg–SiC particulate composite. Compos Part A 2005;36:13–23.
[2] Sawla S, Das S. Combined effect of reinforcement and heat treatment on the two body abrasive wear of aluminum alloy and aluminum particle composites. Wear 2004;257:555–61.
[3] Rosenberger MR, Forlerer E, Schvezov CE. Wear behavior of AA1060 reinforced with alumina under different loads. Wear 2009;266:356–9.
[4] Jiménez AE, Bermúdez MD, Cintas J, Herrera EJ. Dry wear of $NiAl_3$-reinforced mechanically alloyed aluminium with different microstructure. Wear 2009;266:255–65.
[5] Lim CYH, Loe DK, Ang JJS, Gupta M. Wear of magnesium composites reinforced with nano-sized alumina particulates. Wear 2005;259:620–5.
[6] Zhang J, Alpas AT. Wear regimes and transitions in Al_2O_3 particulate reinforced aluminium alloys. Mater Sci Eng, A 1993;161:273–84.
[7] Kok M, Ozdin K. Wear resistance of aluminium alloy and its composites reinforced by Al_2O_3 particles. J Mater Process Technol 2007;183(2–3):301–9.
[8] Ramesh CS, Safiulla M. Wear behavior of hot extruded Al6061 based composites. Wear 2007;263(1–6):629–35.
[9] Wang YQ, Afsar AM, Jang JH, Han KS, Song JI. Room temperature dry and lubricant wear behaviors of Al_2O_{3f}/SiC_p/Al hybrid metal matrix composites. Wear 2010;268(7–8):863–70.
[10] Sahin Y. Wear behavior of aluminium alloy and its composites reinforced by SiC particles using statistical analysis. Mater Des 2003;24(2):95–103.
[11] Ma T, Yamaura H, Koss DA, Voigt RC. Dry sliding wear behavior of cast SiC-reinforced Al MMCs. Mater Sci Eng A 2003;360(1–2):116–25.
[12] Abdollahi A, Alizadeh A, Bahavarndi HR. Dry sliding tribological behavior and mechanical properties of Al 2024-5 wt.% B4C nanocomposite produced by mechanical milling and hot extrusion. Mater Des 2014;55:471–81.
[13] Baradeswaran A, Perumal AE. Influence of B4C on the tribological and mechanical properties of Al 7075-B4C composites. Compos Part B 2013;54:146–52.
[14] Zhao M, Wu GH, Jiang LT, Dou ZY. Friction and wear properties of TiB_{2P}/Al composite. Compos Part A 2006;37(11):1916–21.
[15] Mandal A, Murty BS, Chakraborty M. Wear behaviour of near eutectic Al–Si alloy reinforced with in-situ TiB_2 particles. Mater Sci Eng, A 2009;506:27–33.
[16] Baskaran S, Anandakrishnan V, Duraiselvam M. Investigations on dry sliding wear behavior of in situ casted AA 7075-TiC metal matrix composites by using Taguchi technique. Mater Des 2014;60:184–92.
[17] Jerome S, Ravisankar B, Mahato PK, Natarajan S. Synthesis and evaluation of mechanical and high temperature tribological properties of in-situ Al–TiC composites. Tribol Int 2010;43:2029–36.
[18] Patnaik A, Satapathy A, Mahapatra SS, Dash RR. Tribo-performance of polyester hybrid composites: damage assessment and parameter optimization using Taguchi design. Mater Des 2009;30:57–67.
[19] Ahlatchi H, Kocer T, Candan E, Cimenoglu H. Wear behaviour of Al/(Al_2O_{3p} + SiC_p) hybrid composites. Tribol Int 2006;39:213–20.
[20] Gurcan AB, Baker TN. Wear behaviour of AA 6061 aluminum alloy and its composites. Wear 1995;188:185–91.
[21] Park HC. Wear behaviour of hybrid metal matrix composite materials. Scr Metall Mater 1992;27:465–70.
[22] Mohammed Sharifi E, Karimzadeh F. Wear behaviour of aluminium matrix hybrid nanocomposites fabricated by powder metallurgy. Wear 2011;271:1072–9.
[23] Suresha S, Sridhara BK. Effect of addition of graphite particulates on the wear behaviour on aluminium–silicon carbide–graphite composites. Mater Des 2010;31:1804–12.
[24] Ravindran P, Manisekar K, Narayanasamy P, Selvakumar N, Narayanasamy R. Application of factorial techniques to study the wear of Al hybrid composites with graphite addition. Mater Des 2012;39:42–54.
[25] Ravindran P, Manisekar K, Narayanasamy R, Narayanasamy P. Tribological behaviour of powder metallurgy-processed aluminium hybrid composites with the addition of graphite solid lubricant. Ceram Int 2013;39:1169–82.
[26] Umanath K, Palanikumar K, Selvakumar ST. Analysis of dry sliding wear behaviour of Al 6061/SiC/Al_2O_3 hybrid metal matrix composites. Compos Part B 2013;53:159–68.
[27] Jeyasimman D, Sivasankaran S, Sivaprasad K, Narayanasamy R, Kambali RS. An investigation of synthesis, consolidation and mechanical behaviour of Al 6061 nanocomposites reinforced by TiC via mechanical alloying. Mater Des 2014;57:394–404.
[28] Jeyasimman D, Sivaprasad K, Sivasankaran S, Ponalugusamy R, Narayanasamy R, Vijay Kumar Iyer. Microstructural observation, consolidation and mechanical behaviour of AA 6061 nanocomposites reinforced by γ-Al_2O_3 nanoparticles. Adv Powder Technol [in preparation].
[29] Jeyasimman D, Sivasankaran S, Sivaprasad K, Ponalagusamy R, Narayanasamy R. Role of nanolevel reinforcement on microstructural observation, characterization and consolidation behavior of AA 6061 nanocomposite. Powder Technol [in preparation].
[30] Chowdhury MA, Khalil MK, Nuruzzaman DM, Rahaman ML. The effect of sliding speed and normal load on friction and wear property of aluminum. Int J Mech Mech Eng 2011;11(1):45–9.
[31] Basavarajappa S, Chandramohan G, Paulo Davim J. Application of Taguchi techniques to study dry sliding wear behaviour of metal matrix composites. Mater Des 2007;28:1393–8.
[32] Selvam B, Marimuthu P, Narayanasamy R, Anandakrishnan V, Tun KS, Gupta M, et al. Dry sliding wear behaviour of zinc oxide reinforced magnesium matrix nano-composites. Mater Des 2014;58:475–81.
[33] ASTM standard test method for wear testing with a Pin-on-Disc apparatus. ASTM G 99-95. Philadelphia, PA; 1995.
[34] Rao RN, Das S. Effect of sliding distance on the wear and friction behavior of as cast and heat-treated Al–SiCp composites. Mater Des 2011;32:3051–8.
[35] Mazahery A, Shabani MO. Study on microstructure and abrasive wear behavior of sintered Al matrix composites. Ceram Int 2012;38:4263–9.
[36] Hokkirigawa K, Kato K. An experimental and theoretical investigation of ploughing, cutting and wedge formation during abrasive wear. Tribol Int 1988;21:51–7.
[37] Suh NP. The delamination theory of wear. Wear 1973;25:111–24.
[38] Lim CYH, Lim SC, Gupta M. Wear behavior of SiC_p-reinforced magnesium matrix composites. Wear 2003;255:629–37.
[39] Ahlatchi H, Kocer T, Candan E, Cimenoglu H. Wear behavior of Al/(Al_2O_{3p}-SiC_p) hybrid composites. Tribol Int 2006;39:213–20.
[40] Babu JSS, Kang CG, Kim HH. Dry sliding wear behavior of aluminum based hybrid composites with graphite nanofiber–alumina nanofiber. Mater Des 2011;32:3920–5.